Observation of spectral modulation coupled with broadband transverse-mode-locking in an Yb:CALGO frequency-degenerate cavity

Yijie Shen (申艺杰), Zhensong Wan (万震松), Xing Fu (付 星)*, and Mali Gong (巩马理)

State Key Laboratory of Precision Measurement Technology and Instruments, Department of Precision Instrument, Tsinghua University, Beijing 100084, China

**Corresponding author: fuxing@mail.tsinghua.edu.cn*

Received August 29, 2018; accepted December 27, 2018; posted online March 7, 2019

A frequency-degenerate cavity (FDC) is the resonator that the ratio of transverse and longitudinal mode frequency spacings is a simple rational number. When an optical resonator is close to the FDC, transverse-mode-locking (TML) takes place with drastic changes of laser mode. We report for the first time, to the best of our knowledge, the multi-frequency emission and spectral modulation effects coupled with TML in FDC. The Yb:$CaGdAlO_4$ (Yb:CALGO) crystal with large gain bandwidth was used as a gain medium in an off-axis-pumped hemispherical FDC for realizing broadband emission. Interestingly, the spectrum can transform from a single smooth packet shape to a multi-peak structure; meanwhile, the transverse pattern accordingly transforms into some exotic wave-packet profiles through controlling off-axis displacement in a special degenerate state.

OCIS codes: 140.3410, 140.3518, 140.3580.

doi: 10.3788/COL201917.031404.

To fulfill the reentrant condition of a two-dimensional coupled harmonic oscillator in special unity SU(2) Lie algebra, the cavity configuration requires a frequency-degeneracy state (FDS) of $\Delta f_T/\Delta f_L = P/Q$, where P and Q are coprime integers, and Δf_T (Δf_L) is the longitudinal (transverse) mode spacing[1,2]. The optical resonator satisfying the FDS is called the frequency-degenerate cavity (FDC). The fraction $\Omega = P/Q = (1/\pi)\arccos(\sqrt{1-L/R})$ reveals the degeneracy in a plano–concave cavity with the length of L and radius of curvature of R. When an off-axis-pumped laser resonator is close to the FDC, the laser modes have a preference to be localized on the periodic ray trajectories in contrast to conventional high-order modes, which are called the ray-wave duality (RWD)[1]; meanwhile, the output powers can be drastically increased with the appearance of the periodic ray paths due to the occurrence of the mode degeneracy[1,3]. The RWD effect becomes more distinct with the fraction Ω being close to a simpler fraction of coprime integers and with a larger off-axis displacement[1]. Since the rational number field $\mathbb{Q}$ is dense and countable, the cavity parameters for the emergence of RWD near FDS can form a devil's staircase[4]. These salient properties have hatched many intriguing physical phenomena, such as emitting exotic transverse patterns of three-dimensional (3D) Lissajous parametric surfaces[2,4,5], quantum Green's functions[6,7], and vortex beams with large orbital angular momentum (OAM)[3,8] via FDC. Recently, the self-starting longitudinal-mode-locking (LML) pulses were generated in FDC, which can obtain multi-path picosecond (ps)-level pulses output with exotic transverse patterns (the pulse duration is about 22 ps with spectrum bandwidth of ~0.1 nm)[8,9].

In contrast to the LML, where the locked temporal phase induces ultrashort pulses, transverse-mode-locking (TML) means the locking of the Gouy phase, which induces peculiar spatial transverse patterns[10]. It has been proved that various exotic transverse patterns in FDC are interpreted by the TML effect[1–9], i.e., the spontaneous process of cooperative frequency-locking. Based on the TML effect, the FDC modes can be represented as a coherent state of the SU(2) wave-packet[11,12]. The geometry of classical periodic orbits in FDC is also proved to be relevant to quantum coherent states by SU(2) group transformations[12]. Therefore, the investigations of TML in FDC can provide valuable insights not only into laser physics but also into relevant mesoscopic quantum phenomena. Though the LML and TML in FDC have been studied[1–12], the TML-coupled spectral modulation features of a broadband frequency-degenerate laser have never been reported.

In this Letter, we originally exploit the multi-frequency emission and spectral modulation effects coupled with TML in an FDC. A new crystal Yb:$CaGdAlO_4$ (Yb:CALGO) was used as the gain medium in a plano–concave FDC for allowing a broadband spectrum output, taking advantage of its extremely large gain bandwidth[13,14]. Besides the large gain bandwidth, Yb:CALGO also possess advantages of high thermal conductivity and low refractive-index-temperature gradient[13,15], which are beneficial to the laser performance and stability. When the cavity was adjusted to the FDS $|\Omega = 1/4\rangle$, the output spectrum could transform from a smooth peak with a bandwidth of 6.2 nm to a multi-peak shape; meanwhile, the transverse pattern transformed to an exotic wave-packet profile under certain off-axis displacement. The multi-peak spectrum

consisted of 2–4 peaks with the maximum spacing of about 1 nm. Note that the spacing between adjacent peaks of the spectrum in this process was not equal to Δf_L (~0.0111 nm) or Δf_T (~0.0028 nm). These peculiar phenomena account for a special broadband TML process with a broadband spectrum. The new spectral modulation effect can inspire new frequency-degenerate theories of broadband or quasi-monochromatic TML, rather than the current monochromatic case. Additionally, it also has great potential for applications of exotic OAM beams, transverse frequency comb, and deeper exploration of the quantum–classical connection.

The laser cavity in our experiment consisted of a plane mirror with antireflection (AR) coated at 976 nm and high-reflection (HR) coated at 1020–1080 nm, as well as a concave output coupling mirror ($R = 100$ mm, transmittance of 1% at 1020–1080 nm). The gain medium was a $4\ \text{mm} \times 4\ \text{mm} \times 2\ \text{mm}$ a-cut 5% (atomic fraction) doped Yb:CALGO crystal, which was AR coated at 976–1080 nm at the front and back surfaces and water-cooled at 18°C in a copper heat sink. The pump source was a 976 nm fiber-coupled laser diode (Han's TCS, core: 105 μm, NA: 0.22, highest power: 110 W). The radius of the pump waist was adjusted to approximately 100 μm by a controllable telescope system including two AR-coated lenses. The position of the pump focus spot on the crystal of 100 μm could be precisely controlled. The plane mirror could also be precisely controlled to adjust the cavity length. The laser transverse patterns were captured by a CCD camera (Spiricon, M2-200s) after a focusing lens [Fig. 1(c)]. The spectrum was measured by an optical spectrum analyzer (OSA, Agilent, 86140B) [Fig. 1(d)].

It has been proved that the emission mode in the off-axis-pumped hemispherical FDC is given by the SU(2) wave representation at FDS $|\Omega = P/Q\rangle$[3]:

$$\Psi^{M}_{n_0}(\mathbf{r}, z; \phi) = \sum_{K=n_0}^{M} \binom{M}{K}^{1/2} \frac{e^{\mathrm{i}K\phi}}{2^{M/2}} \Psi^{(\mathrm{HG})}_{n_0+Q\cdot K,0,s_0-P\cdot K}(\mathbf{r}, z), \tag{1}$$

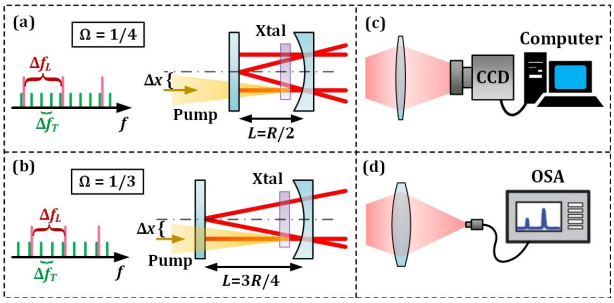

Fig. 1. Schematics of the FDC for the conditions of (a) $|\Omega = 1/4\rangle$ and (b) $|\Omega = 1/3\rangle$; the inserts show the corresponding transverse and longitudinal frequency distributions and periodic ray trajectories. Schematics of the measurements of (c) transverse patterns and (d) spectrum. CCD, charge-coupled device; OSA, optical spectrum analyzer; Xtal, crystal.

where $\mathbf{r} = (x, y)$, ϕ is the locked Gouy phase induced by TML, $M + 1$ represents the number of the decomposed Hermite–Gaussian (HG) modes, and n_0 and s_0 represent the minimum transverse and maximum longitudinal orders, respectively.

$$\Psi^{(\mathrm{HG})}_{n,m,s}(\mathbf{r}, z) = \frac{C^{(\mathrm{HG})}_{n,m}}{w(z)} H_n\left[\frac{\sqrt{2}x}{w(z)}\right] H_m\left[\frac{\sqrt{2}x}{w(z)}\right] \exp\left[\frac{-|\mathbf{r}|^2}{w^2(z)}\right] \times \exp[\mathrm{i}k_{n,m,s}\tilde{z} - \mathrm{i}(m + n + 1)\theta(z)], \tag{2}$$

where $C^{(\mathrm{HG})}_{n,m}$ is the normalized coefficient, $\theta(z) = \arctan(z/z_R)$ is the Gouy phase, $H_n(\cdot)$ represents the Hermite polynomials of the nth order, $k_{n,m,s} = 2\pi f_{n,m,s}/c$, $f_{n,m,s}$ is the eigenmode frequency, c is the speed of light, $\tilde{z} = z + (x^2 + y^2)z/[2(z^2 + z_R^2)]$, $w(z) = w_0\sqrt{1 + (z/z_R)^2}$, $w_0 = \sqrt{\lambda z_R/\pi}$ is the beam radius at the waist, and λ is the emission wavelength. The eigenmode frequency of the resonator can be given by $f_{n,m,s} = s \cdot \Delta f_L + (n + m + 1) \cdot \Delta f_T$, where $\Delta f_L = c/(2L)$ and $\Delta f_T = \Delta f_L \theta(L)/\pi$. Enlargement of the off-axis displacement increases the mode orders n_0 and M of the SU(2) mode. The transverse patterns of selective orders at $|\Omega = 1/4\rangle$ and $|\Omega = 1/3\rangle$ are shown in Tables 1 and 2.

We set the cavity length around $L = 50$ mm for reaching the FDS $|\Omega = 1/4\rangle$. The corresponding periodic ray paths are depicted in Fig. 1(a). According to the RWD principle, the transverse pattern would have the profiles of SU(2) wave-packets, as demonstrated in Table 1. However, in our broad-spectrum off-axis-pumped Yb:CALGO laser FDC, novel phenomena were observed. The recorded transverse pattern evolution versus the off-axis displacements (noted as Δx) is shown in Fig. 2(a) (see video in Visualization 1). The pump power was maintained at 24.1 W in the process of varying the off-axis displacement. As can be seen, instead of a normal SU(2) wave-packet, there were several exotic multi-wave-packet profiles (some extrinsic HG modes were mixed). The output was a near-fundamental-transverse-electromagnetic (TEM_{00}) mode as Δx increased from 0 to 200 μm. With $\Delta x \approx 200$ μm, the circular Gaussian shape mode suddenly divided into two bright spots. As Δx continually increased to 240 μm, the pattern was then divided into three bright spots. For $\Delta x \approx 260$ μm, the spots' shape became unobservable, and the pattern looked like a dumb-bell shape with a bridge connecting two main circles. For $\Delta x \approx 350$ μm, the bridge dramatically transformed into multiple sub-circles. As Δx enlarged from 350 to 433 μm, the number of the sub-circles gradually increased. For $\Delta x = 464$ μm, these sub-circles could no longer be distinguished and were transformed into a wave-packet shape, while the main circles at both sides always existed. During the process that Δx was raised from 464 to 618 μm, the envelope of the center wave-packet gradually changed into two symmetrical bumps, and the fringes of the carrier wave of the wave-packet became more complicated. With $\Delta x = 728$ μm, it was difficult to distinguish the envelope

Table 1. SU(2) Wave Representation of Geometric Modes in Off-axis-pumped FDC of $|\Omega = 1/4\rangle$

$\Psi_{n_0}^M(x, y, z; \phi)$	$\phi = 0$	$\phi = \pi/3$	$\phi = 2\pi/3$	$\phi = \pi$
$n_0 = 2, M = 2$	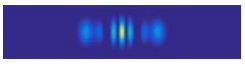	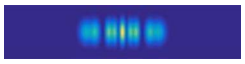	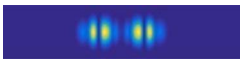	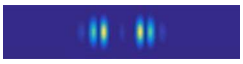
$n_0 = 5, M = 7$		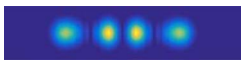	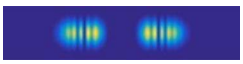	
$n_0 = 10, M = 10$	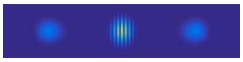	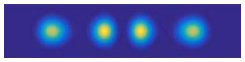		
$n_0 = 18, M = 14$	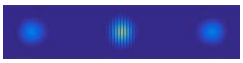	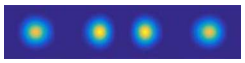		

Table 2. SU(2) Wave Representation of Geometric Modes in Off-axis-pumped FDC of $|\Omega = 1/3\rangle$

$\Psi_{n_0}^M(x, y, z; \phi)$	$\phi = 0$	$\phi = \pi/3$	$\phi = \pi/2$	$\phi = 2\pi/3$
$n_0 = 2, M = 2$	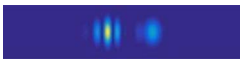	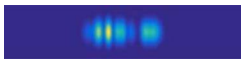	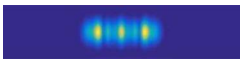	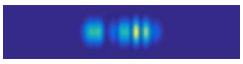
$n_0 = 5, M = 7$		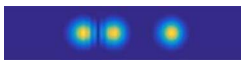	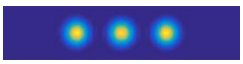	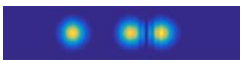
$n_0 = 10, M = 10$		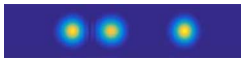	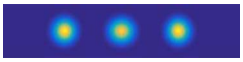	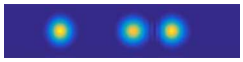
$n_0 = 18, M = 14$		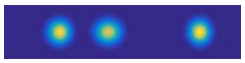	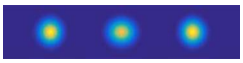	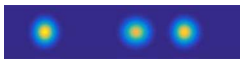

of the wave-packet, while the pattern looked like an aberrant high-order HG mode. As Δx increased from 728 to 812 μm, the observable dual-bump envelope of the wave-packet revisited with a larger size, while the inner fringes continually got more complicated. As Δx was larger than 812 μm, interestingly, the two main circles were no longer distinguished at the sides, while the pattern as a whole changed into a dual-bump wave-packet. Eventually, as Δx went up from 728 to 1080 μm, the portions of the two bumps of the envelope appeared more and more distinctive, while there were no drastic changes until the mode field vanished into nothing.

In previous reports, the measured optical spectra were confirmed as single-peak shapes because the adopted crystals possess narrow gain bandwidth [Nd:YVO_4[1,2,4,9] and Nd:$Y_3Al_5O_{12}$ (Nd:YAG)[3]]. The gain bandwidths of the main emission peaks of Nd:YVO_4[16] and Nd:YAG[17] are only about 0.2–0.7 nm; thus, their laser is approaching monochromatic performance. In that case, the transverse pattern formation could be well interpreted by the theoretical results in Tables 1 and 2. A new kind of crystal, Yb:CALGO, was used in our cavity, having a gain bandwidth as large as 80 nm[12,13], the broadest one among all Yb^{3+}-doped crystals ever discovered, playing the role of broadband modulator. The salient property of Yb:CALGO allowed about 6.2 nm of the output spectrum in our experiment. Compared with the classical SU(2) wave-packet, the Yb:CALGO broadband degenerate mode can show more extrinsic morphologies. Moreover, we observed the intriguing spectral modulation effect in the mode evolution process. The corresponding spectrum evolution is shown in Fig. 2(a). When Δx was increased from 0 to 725 μm, the measured spectrum showed a smooth peak profile centered at 1057 nm, and the linewidth gradually decreased from 6.2 to 3 nm. With $\Delta x \approx 725$ μm, the emergence of a multi-peak spectral structure was observed. As Δx increased further, the peaks were more and more distinguishable. When Δx was around 1 mm, the spectrum profile could be clearly identified as 2–4 peaks with spacings of about 1 nm. Note that the peak positions are unfixed and random, while the maximum spacing between two adjacent main peaks is around 1 nm, which is approximately 100 times larger than $\Delta f_L \approx 0.0111$ nm (corresponding to $\Delta f_T \approx 0.0028$ nm). The measured value of the peak's spacing is credible because the actual resolution of our OSA was set as 0.06 nm, yet it is difficult to tell if it has even finer structures. According to previous degenerate mode theories, the cooperative coincidence of longitudinal and transverse frequencies plays a crucial role in transverse mode formation with the TML effect. However, the new experimental phenomena reported here have two extrinsic characteristics: (1) the coupled spectral modulation with a multi-peak structure and (2) the exotic transverse pattern evolution.

An intuitive explanation can be given that the variation of effective cavity length induced by enlarged off-axis displacement plays a crucial role in the peculiar phenomena. Although the cavity length $L = 50$ mm can marry the state $|\Omega_0 = 1/4\rangle$, the practical perturbation can possibly motivate vicinal states like $|\Omega_1 = 3/11\rangle$, $|\Omega_2 = 5/19\rangle$, and $|\Omega_3 = 7/27\rangle$ (the ratio P_i/Q_i is approximated to $1/4$, $i = 1, 2, 3$). The diagram of mode frequency

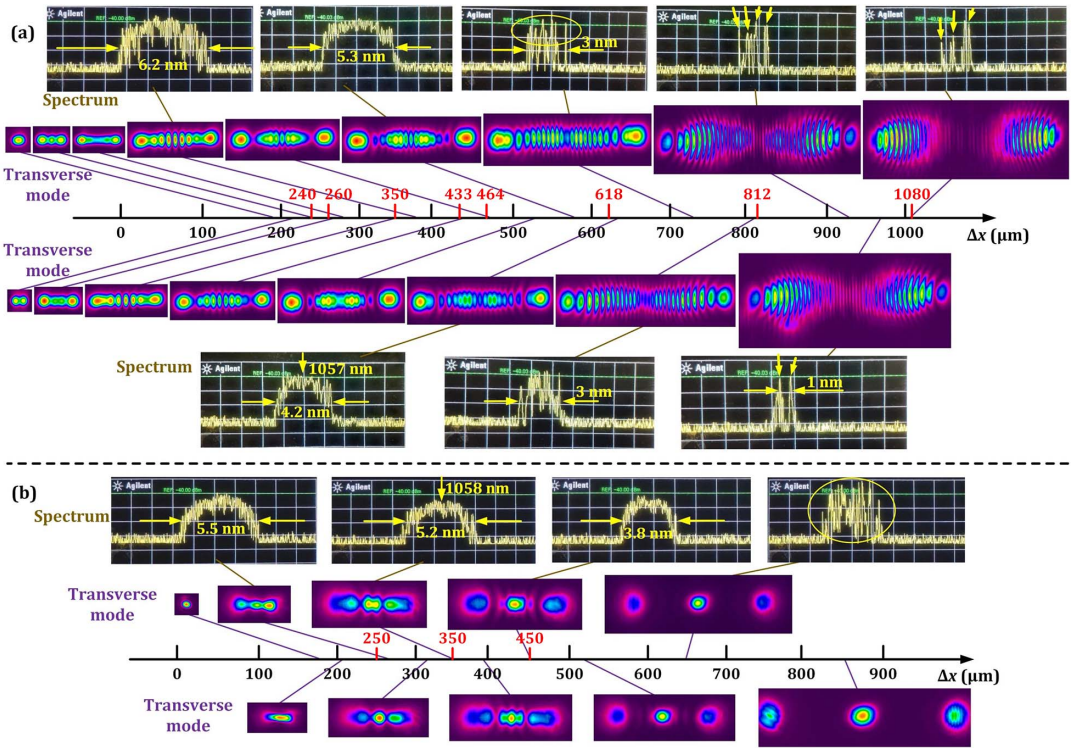

Fig. 2. Recorded transverse patterns and spectral evolutions (see Visualization 3 and Visualization 4) versus the off-axis displacement for (a) $|\Omega = 1/4\rangle$ and (b) $|\Omega = 1/3\rangle$.

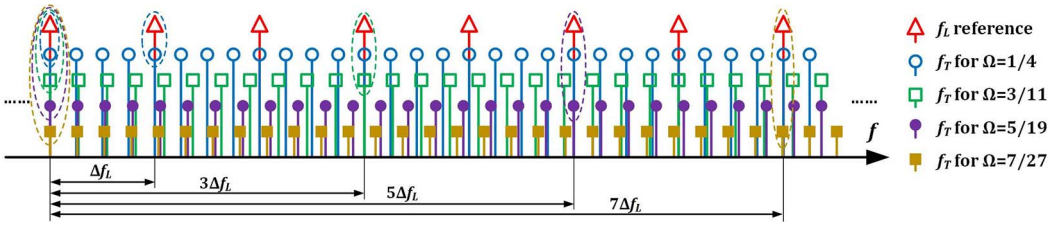

Fig. 3. Diagram of mode frequency distributions, where the dashed circles mark the positions of cooperation of transverse and longitudinal modes corresponding to states $|\Omega_0 = 1/4\rangle$, $|\Omega_1 = 3/11\rangle$, $|\Omega_2 = 5/19\rangle$, and $|\Omega_3 = 7/27\rangle$.

distributions for the above states is depicted in Fig. 3, which illustrates the coherently cooperating relationship among these degenerate states. Then, the actual occurrence of simultaneous cooperation of transverse and longitudinal modes is decided by the lowest common multiple (LCM) of $\{P_0, P_1, P_2, P_3\}$ (hereinafter, the symbol $\{a, b, c, ...\}$ represents the LCM of $a, b, c, ...$). Thus, the most strengthened corporation modes would occur for each spacing of $\{P_0, P_1, P_2, P_3\} \cdot \Delta\lambda_L = \{1, 3, 5, 7\} \cdot \Delta\lambda_L = 105\Delta\lambda_L \approx 1.17$ nm, which agrees with the value of the actually observed maximum peak spacing. For further verifying this explanation, we made the corresponding simulations of the mixed degenerate states, as shown in Fig. 4. As can be seen, the mixed degenerate states have some extrinsic strips structures, which show more agreement with the actual transverse patterns rather than the normal degenerate states. According to the principle of the devil's staircase[4], there can be infinitely many states existed in the vicinity of $|\Omega = 1/4\rangle$, while the states with more complex rational numbers are more difficult to work. Therefore, the actual emitting state can be a more complex mixed state in our Yb:CALGO FDC, yet some tiny corporative degenerate mode spacings beyond the resolution of our device cannot be detected. Additionally, the extrinsic sub-states can introduce the exotic wave-packet transverse patterns. We stress that more rigorous theories should be promoted for interpreting the whole phenomenon in further works. According to our theory, it is also possible that $\{1, 5, 7\}\ \Delta\lambda_L$ (0.39 nm) spacing structure exists in the spectrum. However, on one hand, the 0.39 nm spacing structure can be submerged in the giant ~1 nm spacing structure, which does not lead the contradiction to the above explanation. On the other hand, the 0.39 nm structure is more difficult to be experimentally detected than the ~1 nm structure.

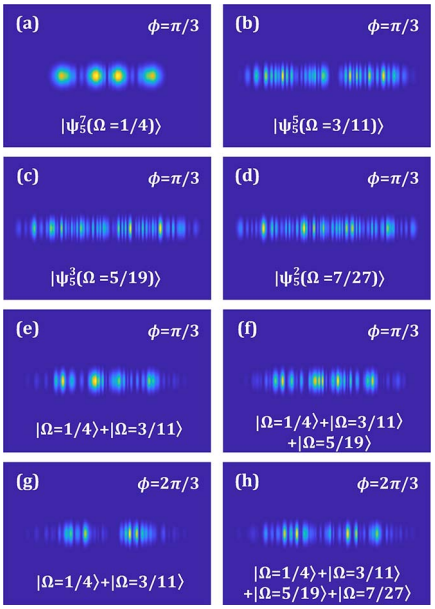

Fig. 4. Simulated results of intensity patterns of degenerate states of (a) $|\Psi_5^7(\Omega=1/4)\rangle$, (b) $|\Psi_5^5(\Omega=3/11)\rangle$, (c) $|\Psi_5^3(\Omega=5/19)\rangle$, and (d) $|\Psi_5^2(\Omega=7/27)\rangle$ when $\phi=\pi/3$; the mixed states of (e) $|\Omega=1/4\rangle+0.5|\Omega=3/11\rangle$, (f) $|\Omega=1/4\rangle+0.5|\Omega=3/11\rangle+0.5|\Omega=5/19\rangle$ when $\phi=\pi/3$; and the mixed states of (g) $|\Omega=1/4\rangle+0.5|\Omega=3/11\rangle$, (h) $|\Omega=1/4\rangle+0.5|\Omega=3/11\rangle+0.5|\Omega=5/19\rangle+0.5|\Omega=7/27\rangle$ when $\phi=2\pi/3$.

When the cavity length was set as $L=75$ mm, FDS $|\Omega=1/3\rangle$ was obtained. The corresponding RWD periodic ray paths with the period of three are depicted in Fig. 1(b). In the experiment, when $\Delta x\approx 250$ μm, the transverse pattern with three bright spots emerged. For Δx in the range from 350 to 450 μm, the wave-packet structure could also be faintly observed. The recorded evolution in this process is shown in Fig. 2(b) (see Visualization 2). In the state $|\Omega=1/3\rangle$, the spectral linewidth is decreasing from 5.5 to 3.8 nm with the increase of Δx. The spectral modulation effect is not as obvious as that in the $|\Omega=1/4\rangle$ state, as shown in Fig. 2(b). Considering that the radius of curvature of $R=100$ mm used here is a larger size than that used in our experiment compared with conventional reports ($R=10$ mm[2,4,8], 20 mm[7], 30 mm[1,3,5]), the $|\Omega=1/3\rangle$ here requires a generally longer cavity length difference (25 mm longer than that of $|\Omega=1/4\rangle$), while the longitudinal mode spacing becomes much shorter (7.4 pm), and the cavity loss is increasing. On one hand, because the longitudinal mode spacing in $|\Omega=1/3\rangle$ became much shorter, the cooperation between transverse and longitudinal modes is less observable in comparison with that in $|\Omega=1/4\rangle$. On the other hand, the increasing loss can reduce some longitudinal modes and narrow the spectral linewidth more, approaching the monochrome emission. Therefore, the emission in $|\Omega=1/3\rangle$ showed near-classical modes in contrast to that in $|\Omega=1/4\rangle$.

Additionally, we did not observe the temporal pulses in the whole process, and the laser was measured as a near continuous wave. In the Nd:YVO_4 FDC, the self-starting LML pulses can be generated due to the self-Kerr-lens effect[8,9], but we did not observe the similar temporal modulation effect. In previous studies of LML, the longitudinal mode is directly impacting on the spectrum, and the temporal signal has a Fourier relation with the spectral signal; the principle is widely demonstrated in the fields of chirped pulses and ultrafast optics. In comparison, our work here demonstrates that the transverse mode can also modulate the spectrum in the broadband TML process. We note that this is understandable because the nonlinear coefficient of Yb:CALGO ($n_2=9\times10^{-20}$ m^2/W)[18] is much less than that of the commonly used Nd:YVO_4 crystal ($n_2=4.7\times10^{-18}$ m^2/W)[19]. Therefore, the spectral modulation effect can be confirmed to be coupled with the spatial TML effect rather than the temporal LML effect.

Conclusively, we report an exotic spectral modulation coupled with the TML effect in an Yb:CALGO FDC. The output spectrum in the $|\Omega=1/4\rangle$ state under certain off-axis displacements can demonstrate an observable multi-peak spectrum with 2–4 peaks with the maximum spacing of about 1 nm. Additionally, the transverse mode can transform into various exotic profiles in contrast to the single-frequency RWD SU(2) wave-packet. In the $|\Omega=1/3\rangle$ state, the extrinsic wave-packet pattern and spectral modulation effects are weaker than those in the $|\Omega=1/4\rangle$ state. The novel spectral modulation effect has vast potential in various applications, such as producing exotic vortex beams with large OAM with a special spectrum and exploring a deeper theory of the SU(2) quantum–classical connection. It is also of high possibility to realize temporal related modulation in this special TML effect and induce novel effects such as transverse frequency comb (a series of discrete, equally spaced transverse mode frequency lines with stable envelope phase) and spatiotemporal-mode-locking pulses in the future.

This work was funded by the National Key Research and Development Program of China (No. 2017YFB1104500), the Natural Science Foundation of Beijing Municipality (No. 4172030), and the Beijing Young Talents Support Project (No. 2017000020124G044).

References

1. Y. F. Chen, J. C. Tung, P. Y. Chiang, H. C. Liang, and K. F. Huang, Phys. Rev. A **88**, 013827 (2011).
2. Y. F. Chen, K. F. Huang, and Y. P. Lan, Opt. Lett. **28**, 1811 (2003).
3. P. H. Tuan, H. C. Liang, K. F. Huang, and Y. F. Chen, IEEE J. Sel. Top. Quantum Electron. **24**, 1600809 (2018).
4. Y. F. Chen, T. H. Lu, K. W. Su, and K. F. Huang, Phys. Rev. Lett. **96**, 213902 (2006).
5. J. C. Tung, H. C. Liang, Y. C. Lin, K. W. Su, K. F. Huang, and Y. F. Chen, Laser Phys. Lett. **11**, 125806 (2014).
6. Y. F. Chen, J. C. Tung, P. H. Tuan, H. C. Liang, and K. F. Huang, Phys. Rev. E **95**, 012217 (2017).
7. J. C. Tung, Y. H. Hsieh, T. Omatsu, K. F. Huang, and Y. F. Chen, Photon. Res. **5**, 733 (2017).

8. J. C. Tung, T. Omatsu, H. C. Liang, K. F. Huang, and Y. F. Chen, Opt. Express **25**, 22769 (2017).
9. H. C. Liang, T. W. Wu, J. C. Tung, C. H. Tsou, K. F. Huang, and Y. F. Chen, Laser Phys. Lett. **10**, 105804 (2014).
10. P. W. Smith, Appl. Phys. Lett. **13**, 235 (1968).
11. C. H. Chen and C. F. Chiu, Opt. Express **15**, 12692 (2007).
12. Y. F. Chen, Phys. Rev. A **83**, 032124 (2011).
13. F. Pirzio, M. Kemnitzer, A. Guandalini, F. Kienle, S. Veronesi, M. Tonelli, J. A. der Au, and A. Agnesi, Opt. Express **24**, 11782 (2016).
14. Y. Shen, Y. Meng, X. Fu, and M. Gong, Opt. Lett. **43**, 291 (2018).
15. P. Loiko, F. Druon, P. Georges, B. Viana, and K. Yumashev, Opt. Mat. Express **4**, 2241 (2014).
16. G. Turri, H. P. Jenssen, F. Cornacchia, M. Tonelli, and M. Bass, J. Opt. Soc. Am. B **26**, 2084 (2009).
17. Y. Sato and T. Taira, Opt. Mat. Express **1**, 514 (2011).
18. S. Manjooran and A. Major, Opt. Lett. **43**, 2324 (2018).
19. J. Guan, X. Li, G. Cheng, G. Chen, and X. Hou, Acta Photon. Sin. **34**, 1172 (2005).